scientific reports

OPEN

Development and validation of radiomics model for MRI-based identification of anterior talofibular ligament injuries

Tian-Xin Chen[1,4], Jun-Ying Wu[1,4], Tong-Jie Yang[2,4], Gang Chen[3], Yan Li[1] & Lei Zhang[1]✉

Anterior talofibular ligament (ATFL) injuries are common ankle injuries that require accurate grading for effective treatment planning. However, conventional diagnostic methods, including manual MRI interpretation, often lack objectivity and reproducibility. Radiomics, a technique that extracts quantitative features from medical images, offers a promising solution for enhancing diagnostic precision. This study developed a radiomics model based on MRI fat-suppressed proton density-weighted turbo spin-echo images to grade ATFL injuries. A dataset of 467 arthroscopically confirmed cases (276 partial tears, 191 complete tears) was analyzed, and 28 key features were selected for model construction using machine learning classifiers. The support vector machine (SVM) model achieved the best performance, with an AUC of 0.955 (95% CI: 0.931–0.980) on the training set and 0.844 (95% CI: 0.781–0.906) on the validation set. Decision curve analysis and confusion matrix results demonstrated the model's strong predictive accuracy and clinical utility. This SVM-based radiomics model offers a reliable, non-invasive approach for precise ATFL injury diagnosis and grading, with significant potential for improving clinical decision-making and personalized treatment.

Keywords Anterior talofibular ligament injury, Magnetic resonance imaging, Radiomics, Machine learning

Ankle sprains represent one of the most prevalent joint injuries, contributing to approximately 40% of all sports-related injuries[1]. Epidemiological studies indicate that ankle sprains have a prevalence of 10% in both males and females, with a notably higher incidence among soccer and basketball players[2,3]. The anterior talofibular ligament (ATFL) is the most frequently injured ligament on the lateral side of the ankle joint. Without timely and appropriate treatment, such injuries can progress to chronic ankle instability (CAI), a condition that significantly affects long-term mobility and quality of life[4]. Studies report that 5–33% of patients with ankle injuries continue to experience pain one year after the initial injury. Moreover, up to 33% of these patients report at least one recurrence, often accompanied by the development of CAI within three years[5]. Therefore, early and accurate diagnosis of ATFL injuries is crucial for effective treatment and prevention of long-term complications.

Clinically, the diagnosis of ankle sprains primarily relies on physical examination, including the anterior drawer and talar tilt tests, supplemented by imaging modalities for confirmation. Among these, ultrasonography has been reported as the most sensitive and specific technique for diagnosing lateral ankle ligament injuries, providing a dynamic, real-time, and cost-effective alternative to magnetic resonance imaging (MRI)[6]. However, MRI remains widely utilized due to its superior soft tissue contrast and accessibility. MRI is well-established as a precise, reliable, and effective imaging modality for evaluating ankle ligament injuries[7]. Studies indicate that MRI demonstrates a sensitivity of 82.1% for acute ATFL injuries and 86.3% for chronic ATFL injuries, highlighting its critical role in the diagnostic workflow of ATFL pathology[8].

In recent years, advancements in artificial intelligence and medical imaging technologies have propelled the emerging field of radiomics into widespread clinical applications. Radiomics focuses on the high-throughput extraction of quantitative features from medical images, enabling the development of models for disease diagnosis and therapeutic efficacy assessment[9]. In this study, we developed a radiomics-based predictive model leveraging MRI data to assess its clinical utility in diagnosing ATFL injuries.

[1]Department of Sports Medicine, Wangjing Hospital of China Academy of Chinese Medical Sciences, Beijing, China. [2]Department of Bone and Joint, Wangjing Hospital of China Academy of Chinese Medical Sciences, Beijing, China. [3]The First School of Clinical Medicine, Nanchang University, Nanchang, Jiangxi, China. [4]These authors contributed equally: Tian-Xin Chen, Jun-Ying Wu, and Tong-Jie Yang. ✉email: arthroartist@163.com

Data and methods
Study design
This retrospective study was performed in line with the principles of the Declaration of Helsinki and approved by the Medical Ethics Committee of Wangjing Hospital of China Academy of Chinese Medical Sciences (IRB No. WJEC-KT-2021-041-P003), and all patients voluntarily signed an informed consent form. All data used in this study were obtained from the electronic medical records, spanning from May 2019 to September 2024, and were kept strictly confidential. Clinical data, including age, sex, history of ankle sprain, and affected side, were collected for each patient. Patients were classified into an ATFL partial tear group or a complete tear group according to arthroscopic findings[10]. Blinded to the imaging and clinicopathological data, the patients were randomly allocated to either a training set or a validation set in a 7:3 ratio. The Flowchart is shown in Fig. 1.

Inclusion and exclusion criteria
This study retrospectively analyzed transverse fat-suppressed proton density-weighted turbo spin-echo (FS-PDw-TSE) of 467 patients with ATFL injuries, confirmed through ankle arthroscopy. Inclusion criteria: (1) between the ages of 18 and 50; (2) ATFL injuries confirmed through arthroscopic examination and identified on 3.0 T MRI scans; (3) complete clinical records; (4) intact cognitive function with ability to cooperate during MRI procedures. Indications for arthroscopy: (1) chronic or recurrent ankle instability, characterized by recurrent sprains, chronic pain, or functional impairment, that has not improved despite at least 3–6 months of conservative treatment; (2) MRI and physical examination findings indicating a grade 3 ATFL tear (complete rupture) or other intra-articular pathologies, such as cartilage or osteochondral damage, which require surgical confirmation and treatment. Exclusion criteria: (1) prior ipsilateral ligament surgery; (2) conditions such as rheumatoid arthritis, osteoarthritis, ankle fractures, malignant tumors, or other diseases affecting ankle symptoms; (3) severe cardiovascular or other systemic diseases, or contraindications to MRI.

Examination method
A 3.0 T MRI system (Magnetom Skyra, Siemens Healthcare, Erlangen, Germany) was utilized, with patients positioned supine, ensuring the affected ankle joint remained in a naturally straight posture. Imaging was performed using an ankle-specific coil with a transverse FS-PDw-TSE (TR 2,390 ms, TE 48 ms, FOV 180 × 180 mm, spacing between slices 0.3 mm, and slice thickness 3 mm). Based on the imaging characteristics of ATFL and clinical expertise, transverse images provide the clearest visualization of the ligament. Consequently, the grade of ATFL damage was assessed primarily using transverse FS-PDw-TSE, which was the focus of this study[11].

Region of interest segmentation
The region of interest (ROI) was manually segmented layer by layer using 3D Slicer software (Version 5.6.2, https://www.slicer.org). To evaluate the intra- and inter-class correlation coefficients (ICC) for feature extraction, MRI images of 30 patients were randomly selected. Two radiologists independently segmented the ligaments on transverse FS-PDw-TSE to delineate the ROI; after a one-week interval, Physician A re-segmented the ROI for the same 30 patients to assess inter- and intra-observer consistency and repeatability. Physician A then completed the ROI segmentation for the remaining 437 patients. The MRI appearances of ATFL tears at different grades are shown in Fig. 2.

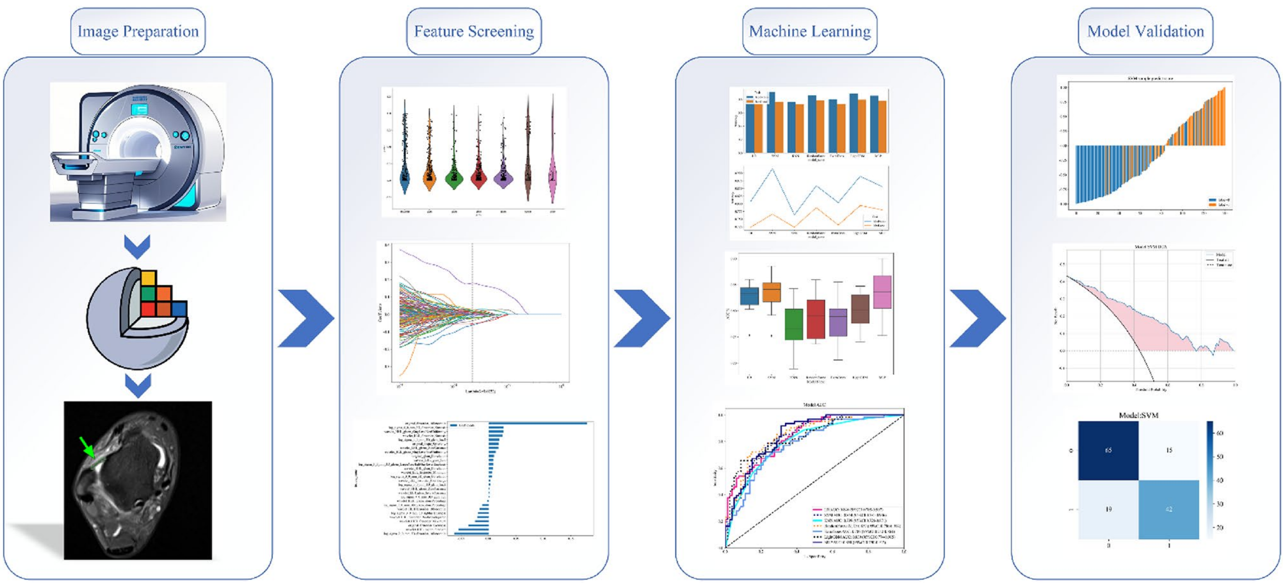

Fig. 1. Flowchart illustrating the study design.

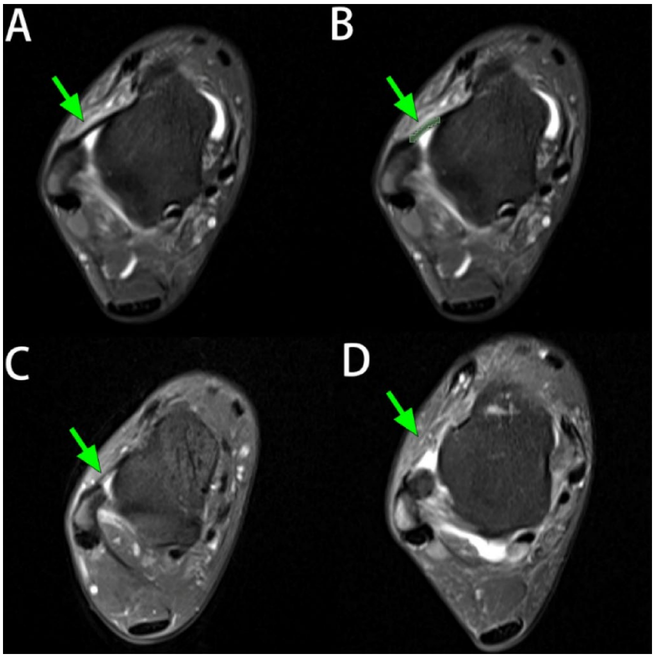

Fig. 2. Sample images for ATFL injuries. (**A**) Normal ATFL. (**B**) ROI outline of ATFL. (**C**) Partial tear of the ATFL. (**D**) Complete tear of the ATFL.

Radiomics feature extraction

Radiomics features were extracted from the manually delineated ROI using PyRadiomics (Version 2.7.7, Python 3.7.3). The extracted radiomics features included the gray-level co-occurrence matrix (GLCM), gray-level size zone matrix (GLSZM), gray-level run-length matrix (GLRLM), neighboring gray-tone difference matrix (NGTDM), gray-level dependence matrix (GLDM), as well as first-order and shape-based features.

Radiomics feature screening

To mitigate the risk of overfitting due to an excessive number of features, data dimensionality reduction and feature screening were systematically conducted in a stepwise manner. Initially, features demonstrating high reproducibility (ICC > 0.75) were retained for subsequent analysis[12]. The process for selecting significant radiomics features involved multiple steps: First, Z-score standardization was applied to normalize feature magnitudes, scaling the data to a mean of 0 and variance of 1. Next, independent sample t-tests were conducted for initial screening, retaining features with $P < 0.05$. Subsequently, Pearson correlation coefficients were calculated for highly reproducible features, retaining those with coefficients greater than 0.9. Finally, the Least Absolute Shrinkage and Selection Operator (LASSO) regression algorithm was employed to identify critical features from each set. Cross-validation and penalty parameter adjustment were used to compress the coefficients of unstable and redundant features to zero, ultimately retaining highly relevant radiomics features with nonzero coefficients[13].

Radiomics models development and validation

The final set of radiomics features was applied using seven machine learning models: Support Vector Machine (SVM), K-Nearest Neighbor, Random Forest, Extra Trees, Light Gradient Boosting Machine, Multilayer Perceptron, and Logistic Regression, to construct radiomics models. Receiver Operating Characteristic (ROC) curves were plotted, and metrics such as the area under the curve (AUC), accuracy, specificity, sensitivity, positive predictive value (PPV), and negative predictive value (NPV) were computed to assess the models' diagnostic performance. The best-performing models were identified based on their AUC values in the validation set. Decision Curve Analysis (DCA) was conducted to assess the clinical utility of the predictive models. A confusion matrix was generated to evaluate the predictive model's accuracy in identifying ATFL injuries.

Statistical analysis

Statistical analyses were conducted using Python 3.7.3. Continuous variables were assessed for normality. Data following a normal distribution were reported as mean ± standard deviation (SD) and compared between groups using an independent samples t-test. Non-normally distributed data were expressed as median (interquartile range) and analyzed using the two-sample rank-sum test. Categorical variables were described as frequencies and compared between groups using the chi-square test or Fisher's exact test, as appropriate. A p-value of < 0.05 was considered statistically significant.

Results

General information

A total of 467 patients with ATFL injuries were included in the study. Based on arthroscopic findings, 276 patients were classified into the partial tear group, and 191 were categorized into the complete tear group. The patients were randomly allocated into a training set and a validation set at a ratio of 7:3. The training set consisted of 326 patients, comprising 196 cases of partial tear and 130 cases of complete tear. The validation set included 141 patients, with 80 cases of partial tear and 61 cases of complete tear. No significant differences were observed in baseline characteristics, including gender, age, history of ankle sprain, and affected side, between the two groups ($P > 0.05$), indicating comparability. Refer to Table 1 for detailed baseline characteristics.

Results of screening radiomics features

A total of 1,197 original radiomics features were extracted, comprising 286 GLCM features, 208 GLSZM features, 208 GLRLM features, 65 NGTDM features, 182 GLDM features, 233 first-order features, and 15 shape features, as illustrated in Fig. 3A and B. Features with an ICC > 0.75 were initially screened, resulting in 906 radiomics features, which were subsequently t-tested, yielding 678 features. When applying a Pearson correlation coefficient threshold of 0.9, the feature set was reduced to 201 features. LASSO cross-validation further downscaled the feature set, as depicted in Fig. 3C and D. A final set of 28 features was selected for constructing radiomics models, including 8 GLCM features, 7 GLSZM features, 2 NGTDM features, 10 first-order features, and 1 shape feature, as presented in Fig. 3E.

Radiomics model development and validation

SVM, K-Nearest Neighbor, Random Forest, Extra Trees, Light Gradient Boosting Machine, Multilayer Perceptron, and Logistic Regression machine learning models were employed for constructing and training radiomics models. The performance of these models was evaluated on the training set. The SVM classifier was ultimately chosen to develop the optimal MRI-based radiomics model, as illustrated in Fig. 4. The SVM model achieved an AUC of 0.955 (95% CI: 0.931–0.980) on the training set and 0.844 (95% CI: 0.781–0.906) on the validation set. The AUC, sensitivity, specificity, accuracy, PPV, and NPV for various models on the training and validation sets are detailed in Table 2.

The final selected radiomics features were linearly combined based on their respective coefficient weightings to calculate the rad-score, and radiomics bar graphs were generated. The results demonstrated that the SVM model exhibited strong predictive performance in grading ATFL injuries in both the training and validation sets, as shown in Fig. 5A and B. DCA revealed that the SVM model achieved a high net clinical benefit ratio in both the training and validation sets, as depicted in Fig. 5C and D. Additionally, the confusion matrix was used to test the classification accuracy of the SVM model. The SVM model demonstrated an accuracy of 91.3% (179/196) in diagnosing partial tears and 91.5% (119/130) in identifying complete tears in the training set. In the validation set, the accuracy was 81.3% (65/80) for partial tears and 68.9% (42/61) for complete tears. Detailed results are presented in Fig. 5E and F.

Discussion

ATFL injury is the most common ligament injury in the ankle joint. Without timely treatment, complications such as CAI and cartilage damage may arise[14]. Currently, ATFL injury is primarily diagnosed through physical examination of the ankle joint and imaging studies. While arthroscopy remains the gold standard for diagnosing ATFL injuries, it is an invasive procedure associated with surgical risks, anesthetic complications, and economic burdens, making it unsuitable as a routine diagnostic method[15]. Consequently, MRI is widely utilized for diagnosing ATFL injuries, despite the increasing clinical recognition of ultrasonography as a valuable alternative. MRI enables staging of the injury into partial and complete tears based on ligament continuity, alignment, and adhesion to surrounding tissues[16]. However, challenges arise when ATFL injuries are accompanied by edema, intra-synovial hemorrhage, or coexisting injuries, as well as partial volume effects caused by surrounding adipose tissue, which can obscure the grading of ligament damage. Radiomics, however, allows for the extraction of numerous deep and quantitative imaging features from medical data[17].

Category	Partial tear group ($n = 276$)	Complete tear group ($n = 191$)	P value
Training set ($n = 326$)			
Age (Years)	34.5 ± 10.9	33.6 ± 12.3	0.49
Sex (Male/Female)	104/92	67/63	0.88
Side (Left/Right)	95/101	55/75	0.33
History of ankle sprain (Yes/No)	132/64	82/48	0.84
Validation set ($n = 141$)			
Age (Years)	35.6 ± 12.9	34.8 ± 11.9	0.99
Sex (Male/Female)	44/36	29/32	0.48
Side (Left/Right)	38/42	33/28	0.54
History of ankle sprain (Yes/No)	52/28	37/24	0.76

Table 1. Baseline characteristics of patients.

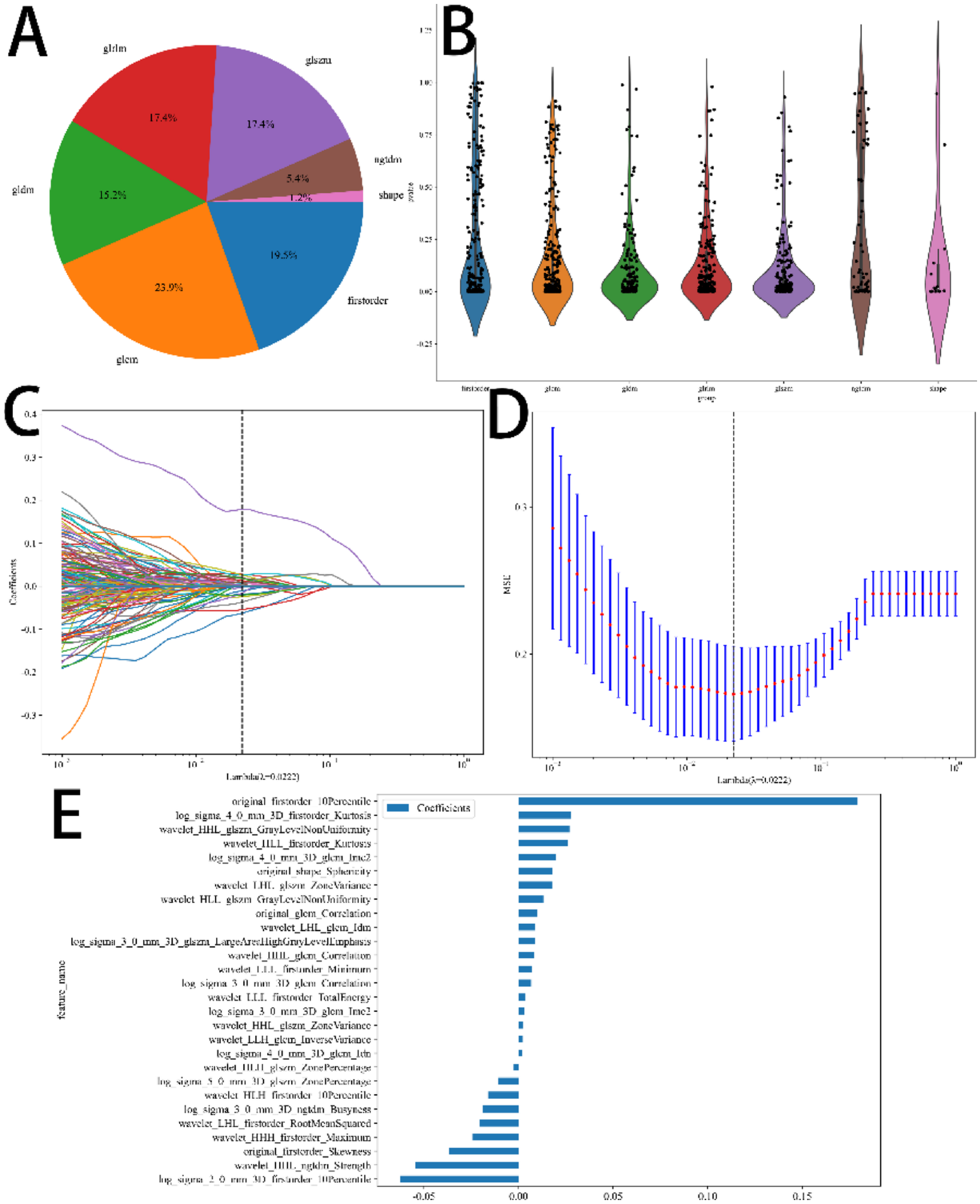

Fig. 3. Radiomics feature screening and results. (**A**) Classification of original radiomics features. (**B**) Distribution of original radiomics features. (**C**) Graph of LASSO 10-fold cross-validation regression. (**D**) Convergence graph of radiomics features of LASSO regression. (**E**) Features used to construct the radiomics model.

In this study, using MRI radiomics techniques, 28 features indicative of ATFL injury were identified, predominantly comprising GLCM, GLSZM, and First-Order features. The GLCM captures the probability distribution of gray-level pairs at specific distances and orientations within an image. GLCM-derived texture features, which are interpretable and effective, have been employed to identify ROI and classify tendinopathy images[18,19]. Additionally, GLCM demonstrates a strong correlation with bone morphometry[20]. This study demonstrates that GLCM plays a vital role in identifying ligament injuries. By quantifying textural features (e.g., contrast, homogeneity) and directional changes in ligament tissues, GLCM sensitively detects microstructural abnormalities, facilitating early diagnosis and treatment efficacy assessment[21]. The GLSZM quantifies the size of pixel regions with the same gray level that are spatially adjacent, capturing the texture consistency and non-periodic characteristics of the image[22]. Ligament injuries often involve structural changes such as edema, fiber disruption, or scar formation[17]. GLSZM effectively quantifies texture consistency and heterogeneity across different regions, enabling the detection of subtle structural alterations. First-order features represent the most fundamental statistical descriptors in radiomics, characterizing pixel intensity distributions within an image, such as mean, standard deviation, skewness, and kurtosis[23]. Unlike texture features, first-order features are independent of spatial relationships and are derived directly from pixel intensity statistics. The mean value

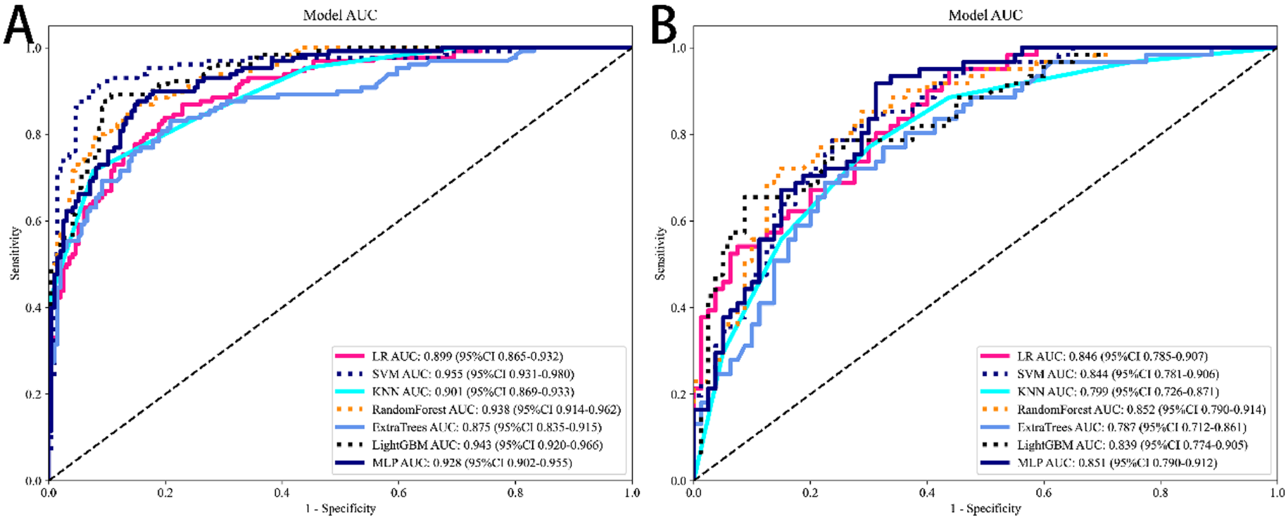

Fig. 4. ROC curves for different machine learning models. (**A**) ROC curve for the training set. (**B**) ROC curve for the validation set; SVM, Support Vector Machine; KNN, K-Nearest Neighbor; LightGBM, Light Gradient Boosting Machine; MLP, Multilayer Perceptron; LR, Logistic Regression.

Model	Group	AUC(95%CI)	Sensitivity	Specificity	Accuracy	PPV	NPV
Support Vector Machine	Train	0.955(0.931-980)	0.915	0.913	0.914	0.875	0.942
Support Vector Machine	Test	0.844(0.781–0.906)	0.770	0.762	0.766	0.712	0.813
K-Nearest Neighbor	Train	0.901(0.869-0933)	0.408	1.000	0.764	1.000	0.718
K-Nearest Neighbor	Test	0.799(0.726–0.871)	0.557	0.850	0.723	0.739	0.716
Random Forest	Train	0.938(0.914–0.962)	0.838	0.872	0.859	0.813	0.891
Random Forest	Test	0.852(0.790–0.914)	0.705	0.850	0.787	0.782	0.791
Extra Trees	Train	0.875(0.835–0.915)	0.823	0.791	0.804	0.723	0.871
Extra Trees	Test	0.787(0.712–0.861)	0.672	0.775	0.730	0.695	0.756
Light Gradient Boosting Machine	Train	0.943(0.920–0.966)	0.885	0.893	0.890	0.846	0.921
Light Gradient Boosting Machine	Test	0.839(0.774–0.905)	0.639	0.912	0.794	0.848	0.768
Multilayer Perceptron	Train	0.928(0.902–0.955)	0.869	0.847	0.856	0.790	0.907
Multilayer Perceptron	Test	0.851(0.790–0.912)	0.902	0.687	0.780	0.687	0.902
Logistic Regression	Train	0.899(0.865–0.932)	0.862	0.770	0.807	0.713	0.893
Logistic Regression	Test	0.846(0.785–0.907)	0.934	0.562	0.723	0.620	0.918

Table 2. Diagnostic performance of various radiomics models in training and validation set. AUC, the area under the curve; PPV, positive predictive value; NPV, negative predictive value.

of first-order features reflects the overall signal intensity of ligaments, which may vary due to injury-related changes such as edema, fibrosis, or other tissue alterations. The standard deviation indicates variations in local density distribution, highlighting increased tissue heterogeneity[24]. In summary, GLCM, GLSZM, and first-order features play a significant role in the diagnosis of ligament injuries.

The findings of this study indicate that the SVM-based radiomics model exhibits high sensitivity, specificity, and net clinical benefit in diagnosing ATFL injuries. SVM is a supervised machine learning algorithm that learns from data to make decisions[25]. The fundamental concept of SVM is to identify a hyperplane that maximizes classification boundaries for optimal separation in binary classification problems. By leveraging the "kernel trick," SVM can handle nonlinear problems by mapping data to a high-dimensional space where it becomes linearly separable[26]. SVM excels in high-dimensional spaces, demonstrating robustness by relying solely on support vector points, thereby avoiding overfitting. It is widely utilized in medical image analysis, anomaly detection, and other fields, serving as a powerful tool in machine learning[27]. SVM is extensively applied in musculoskeletal disorders, with numerous studies focusing on diagnosing and predicting outcomes for injuries such as those of the anterior cruciate ligament[28,29] and the medial patellofemoral ligament[30]. Moreover, its application in diagnosing ankle ligament injuries has gained increasing attention.

Artificial intelligence is increasingly being utilized in the diagnosis of ligament injuries, with machine learning and deep learning methods gaining attention for their potential applications in the assessment of ATFL injuries. Yan W et al.[17] achieved high-accuracy binary classification of ATFL injuries using intelligent localization and SVM. Their method involved feature point extraction with the DRLSE algorithm to locate the

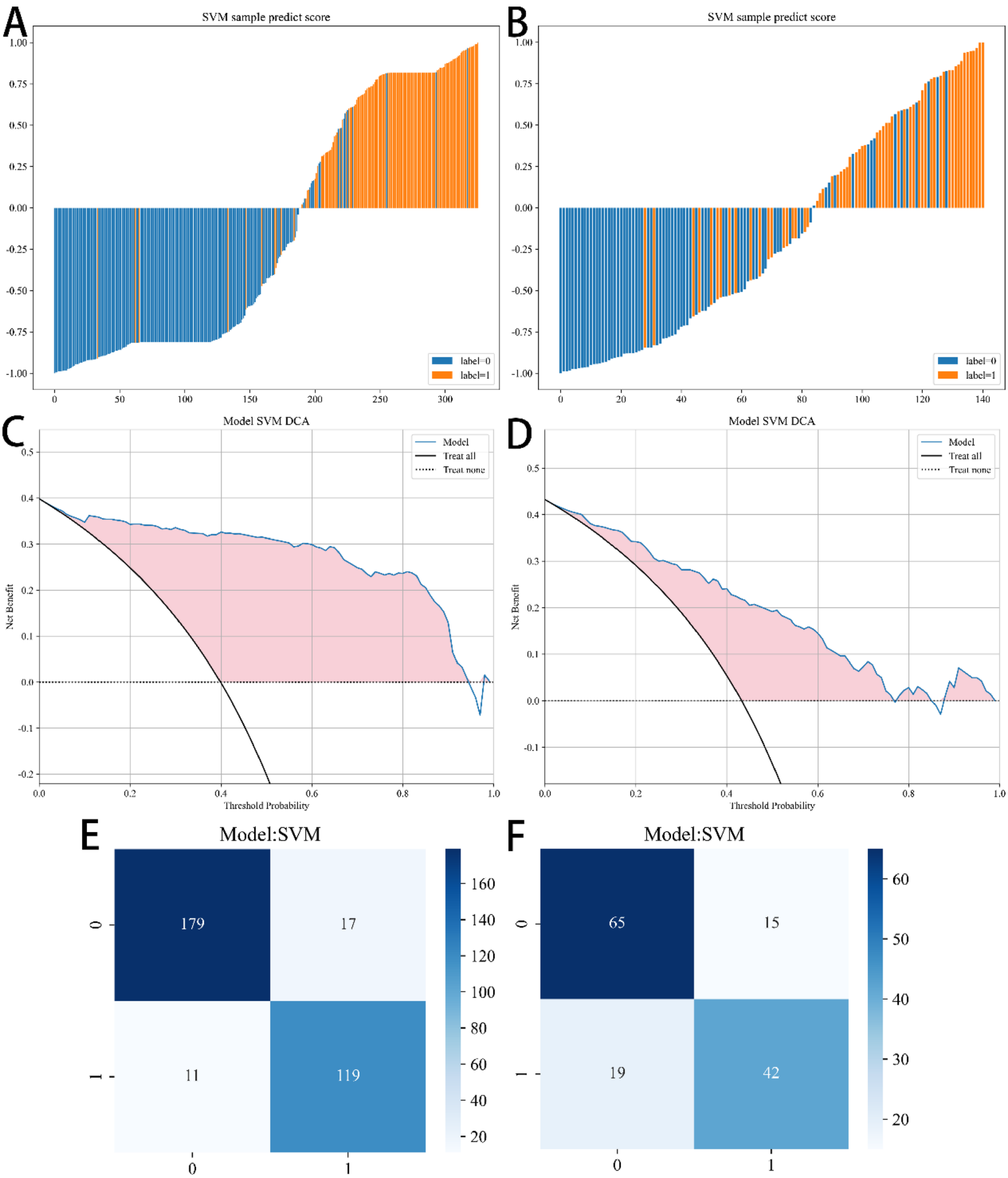

Fig. 5. Radiomics score histograms, DCA curves, and confusion matrices of the SVM model. (**A**) SVM bar graph for the training set. (**B**) SVM bar graph for the validation set. (**C**) DCA curve of the SVM model in the training set. (**D**) DCA curve of the SVM model in the validation set. (**E**) Confusion matrix of the SVM model in the training set. (**F**) Confusion matrix of the SVM model in the validation set.

ATFL region, combined with first-order grayscale and second-order texture features, highlighting its automation and suitability for small sample datasets. This study utilized a larger sample size and a more comprehensive set of radiomics features to develop an SVM model capable of graded diagnosis for partial and complete ATFL tears. Multidimensional evaluation metrics verified the model's predictive efficacy and clinical utility, surpassing existing studies in both diagnostic depth and clinical applicability. Astolfi RS et al.[31] explored small-sample data enhancement and feature extraction techniques to achieve binary classification of ATFL injuries using a random forest classifier. However, their study lacked graded diagnosis, limiting its clinical applicability. This study integrates large-sample multidimensional feature analysis and graded diagnosis, significantly improving the model's accuracy and clinical utility. It offers valuable support for fine-grained diagnosis and optimization of treatment plans for ATFL injuries. Ni M et al.[32] employed a deep learning approach to classify ATFL injuries, utilizing data from 1,073 patients. The model demonstrated superior performance in an external validation cohort, achieving AUCs as high as 0.89–0.99, outperforming radiologists. However, its interpretability remains limited. In contrast, this study leverages radiomics combined with SVM, offering enhanced interpretability that allows clinicians to understand model decisions while providing graded diagnostic support for partial and complete ATFL tears. Additionally, our method is computationally efficient, well-suited for small datasets, and easily deployable in resource-limited healthcare settings. Moreover, we incorporate DCA to quantify the clinical utility of the model, further reinforcing its practical value.

This study has several limitations. First, while this study included imaging data from 467 arthroscopic examinations, it was conducted as a single-center retrospective study. The lack of external validation highlights the need for larger datasets and multicenter sources to enhance the reliability and clinical applicability of radiomics studies. Second, radiomics features in this study were exclusively extracted from transverse FS-PDw-TSE. Future studies should incorporate 3D-MRI, which can provide superior anatomical detail and enhance the accuracy of ligament injury detection[10]. This approach may improve the diagnostic performance and applicability of radiomics-based models. Third, this study primarily analyzed imaging data and did not incorporate clinical characteristics of patients. As a result, predictive models incorporating clinical features were not developed. Future research should integrate clinical data to improve diagnostic and therapeutic strategies for ATFL injuries[33]. Finally, as this was a retrospective study, we could not ensure that all transverse slices were perfectly parallel to the ATFL. Additionally, this study did not exclude individuals with increased lateral ankle laxity due to inadequate initial treatment, nor did it assess its relationship with MRI findings[34].

This study demonstrated excellent diagnostic performance by leveraging MRI-extracted radiomic features and an SVM classifier to construct a predictive model for ATFL injury identification, offering valuable insights into the diagnosis and management of ankle injuries while equipping clinicians with an objective and accurate diagnostic tool.

Data availability

The raw data underlying this study are available from the corresponding author upon reasonable request.

Received: 23 November 2024; Accepted: 23 April 2025
Published online: 04 May 2025

References

1. Choi, Y. H., Cho, S. H., Seo, J. Y., Ahn, J. H. & Kim, Y. C. Apoptosis occurs in the anterior talofibular ligament of patients with chronic lateral ankle instability: an in vitro study. *Clin. Orthop. Relat. Res.* **480**, 2420–2429 (2022).
2. Doherty, C. et al. The incidence and prevalence of ankle sprain injury: a systematic review and meta-analysis of prospective epidemiological studies. *Sports Med.* **44**, 123–140 (2014).
3. Fong, D. T. P., Hong, Y., Chan, L. K., Yung, P. S. H. & Chan, K. M. A systematic review on ankle injury and ankle sprain in sports. *Sports Med.* **37**, 73–94 (2007).
4. Hagio, T., Yoshimura, I., Kanazawa, K., Minokawa, S. & Yamamoto, T. Morphology of anterior talofibular ligament after arthroscopic lateral ankle ligament repair. *Foot Ankle Int.* **41**, 993–1001 (2020).
5. Gribble, P. A. et al. Evidence review for the 2016 international ankle consortium consensus statement on the prevalence, impact and long-term consequences of lateral ankle sprains. *Br. J. Sports Med.* **50**, 1496–1505 (2016).
6. Colò, G., Bignotti, B., Costa, G., Signori, A. & Tagliafico, A. S. Ultrasound or MRI in the evaluation of anterior talofibular ligament (ATFL) injuries: systematic review and Meta-Analysis. *Diagnostics (Basel)*. **13** (14), 1–12 (2023).
7. Casado-Hernández, I. et al. Association between anterior talofibular ligament injury and ankle tendon, ligament, and joint conditions revealed by magnetic resonance imaging. *Quant. Imaging Med. Surg.* **11**, 84–94 (2021).
8. Cao, M. et al. Imaging diagnosis for anterior talofibular ligament injury: a systemic review with meta-analysis. *Acta Radiol.* **64**, 612–624 (2023).
9. Fritz, B., Yi, P. H., Kijowski, R. & Fritz, J. Radiomics and deep learning for disease detection in musculoskeletal radiology: an overview of novel MRI- and CT-Based approaches. *Invest. Radiol.* **58**, 3–13 (2023).
10. Xu, Y., He, L., Han, Y., Duan, D. & Ouyang, L. Evaluation of 3-Dimensional magnetic resonance imaging (3D MRI) in diagnosing anterior talofibular ligament injury. *Med. Sci. Monit.* **7**, e927920 (2021).
11. Cao, S. et al. Reliability and validity of different ankle MRI scanning planes for the anterior talofibular ligament injury diagnosis: a cadaveric study. *J. Orthop. Surg. Res.* **14**, 69 (2019).
12. Abdali, S. H., Afzali, F., Baseri, S., Abdalvand, N. & Abdollahi, H. Bone radiomics reproducibility: a three-centered study on the impacts of image contrast, edge enhancement, and latitude variations. *Phys. Eng. Sci. Med.* **45**, 497–511 (2022).
13. Ye, G. et al. An advanced nomogram model using deep learning radiomics and clinical data for predicting occult lymph node metastasis in lung adenocarcinoma. *Transl Oncol.* **44**, 101922 (2024).
14. Zhang, L. et al. The increased anterior talofibular ligament-posterior talofibular ligament angle on MRI May help evaluate chronic ankle instability. *Surg. Radiol. Anat.* **45**, 1205–1211 (2023).
15. Han, J. et al. Modified classifications and surgical decision-making process for chronic anterior talofibular ligament injuries based on the correlation of imaging studies and arthroscopic findings. *Int. Orthop.* **47**, 2683–2692 (2023).
16. Joshy, S., Abdulkadir, U., Chaganti, S., Sullivan, B. & Hariharan, K. Accuracy of MRI scan in the diagnosis of ligamentous and Chondral pathology in the ankle. *Foot Ankle Surg.* **16**, 78–80 (2010).
17. Yan, W., Meng, X., Sun, J., Yu, H. & Wang, Z. Intelligent localization and quantitative evaluation of anterior talofibular ligament injury using magnetic resonance imaging of ankle. *BMC Med. Imaging.* **21**, 130 (2021).
18. Scott, I. et al. An automated method for tendon image segmentation on ultrasound using grey-level co-occurrence matrix features and hidden Gaussian Markov random fields. *Comput. Biol. Med.* **69**, 107872 (2024).
19. Schneebeli, A. et al. Test-retest reliability of echo intensity parameters in healthy Achilles tendons using a semi-automatic tracing procedure. *Skeletal Radiol.* **46**, 1553–1558 (2017).
20. Orhan, K., Driesen, L., Shujaat, S., Jacobs, R. & Chai, X. Development and Validation of a Magnetic Resonance Imaging-Based Machine Learning Model for TMJ Pathologies. *Biomed. Res. Int.* 6656773 (2021). (2021).
21. Haralick, R. M., Shanmugam, K. & Dinstein, I. Textural features for image classification. *IEEE Trans. Syst. Man. Cybern*. **3**, 610–621 (1973).

22. Thibault, G. et al. Texture Indexes and Gray Level Size Zone Matrix: Application to Cell Nuclei Classification. *In Proceedings of the 10th International Conference on Pattern Recognition and Information Processing (PRIP* 140–145 (2009). (2009).
23. Varriano, G., Guerriero, P., Santone, A., Mercaldo, F. & Brunese, L. Explainability of radiomics through formal methods. *Comput. Methods Programs Biomed.* **220**, 106824 (2022).
24. Doshi, A. M. et al. Assessment of renal cell carcinoma by texture analysis in clinical practice: A Six-Site, Six-Platform analysis of reliability. *AJR Am. J. Roentgenol.* **217**, 1132–1140 (2021).
25. Valkenborg, D., Rousseau, A. J., Geubbelmans, M. & Burzykowski, T. Support vector machines. *Am. J. Orthod. Dentofac. Orthop.* **164**, 754–757 (2023).
26. Borstelmann, S. M. Machine learning principles for radiology investigators. *Acad. Radiol.* **27**, 13–25 (2020).
27. Liang, Y., Bo, K., Meyyappan, S. & Ding, M. Decoding fMRI data with support vector machines and deep neural networks. *J. Neurosci. Methods.* **01**, 110004 (2024).
28. Chen, D. S. et al. A novel application of unsupervised machine learning and supervised machine learning-Derived radiomics in anterior cruciate ligament rupture. *Risk Manag Healthc. Policy*. **4**, 2657–2664 (2021).
29. Flannery, S. W. et al. Predicting anterior cruciate ligament failure load with T2* relaxometry and machine learning as a prospective imaging biomarker for revision surgery. *Sci. Rep.* **13**, 3524 (2023).
30. Zhan, H. et al. Machine-Learning models reliably predict clinical outcomes in medial patellofemoral ligament reconstruction. *Arthroscopy* https://doi.org/10.1016/j.arthro.2024.07.028 (2024).
31. Astolfi, R. S. et al. Computer-Aided ankle ligament injury diagnosis from magnetic resonance images using machine learning techniques. *Sens. (Basel).* **23**, 1–18 (2023).
32. Ni, M., Chen, W., Zhao, Q., Zhao, Y. & &Yuan, H. Deep learning approach for MRI in the classification of anterior talofibular ligament injuries. *J. Magn. Reson. Imaging.* **58**, 1544–1556 (2023).
33. Zhang, J. et al. Risk factors for chronic ankle instability after first episode of lateral ankle sprain: A retrospective analysis of 362 cases. *J. Sport Health Sci.* **12**, 606–612 (2023).
34. Chen, R. P. et al. Progress in diagnosis and treatment of acute injury to the anterior talofibular ligament. *World J. Clin. Cases*. **11**, 3395–3407 (2023).

Acknowledgements
We gratefully acknowledged the radiologists who were involved in the study.

Author contributions
T.X.C., J.Y.W., and T.J.Y. conceptualized the study, conducted data curation and investigation, developed the methodology, and contributed to writing the original draft as well as reviewing and editing the manuscript. G.C. and Y.L. participated in data curation and investigation and contributed to reviewing and editing the manuscript. L.Z. provided conceptualization, methodology, and supervision, and contributed to funding acquisition and reviewing and editing the manuscript. All authors reviewed and approved the final manuscript.

Funding statement
This work was supported by the China Academy of Chinese Medical Sciences Innovation Fund (No. CI2021A02009).

Declarations

Competing interests
The authors declare no competing interests.

Date statement
The work has been approved by the appropriate ethical committees related to the institution(s) in which it was performed and has obtained written informed consent from the study participants.

Ethics statement
This study was performed in line with the principles of the Declaration of Helsinki and approved by the Medical Ethics Committee of Wangjing Hospital of China Academy of Chinese Medical Sciences (IRB No. WJEC-KT-2021-041-P003), and all patients voluntarily signed an informed consent form.

Additional information
Correspondence and requests for materials should be addressed to L.Z.